High-Precision ZTD Model of Altitude-Related Correction

Qingzhi Zhao, Jing Su, Chaoqian Xu, Yibin Yao, Xiaoya Zhang, and Jifeng Wu

Abstract—Zenith tropospheric delay (ZTD) is one of the main error sources in space geodesy. The existing regional or global models, such as Global Pressure and Temperature 3 (GPT3), Global Tropospheric model, Global Hopfield, and Shanghai Astronomical observatory tropospheric delay model models, have good performance. However, the precision of these models is relatively low in regions with a large height difference, which becomes the focus of this article. A high-precision ZTD model considering the height effect on tropospheric delay is proposed, and China is selected as study area due to its large height difference, which is called the high-precision ZTD model for China (CHZ). The initial ZTD value is calculated on the basis of the GPT3 model, and the periodic terms of ZTD residual between the global navigation satellite system (GNSS) and GPT3 model, such as annual, semiannual, and seasonal periods, are determined by the Lomb–Scargle periodogram method in different subareas of China. The relationship between the ZTD periodic residual term and the height of the GNSS station is further analyzed at different seasons, and linear ZTD periodic residual models are obtained. A total of 164 GNSS stations derived from the Crustal Movement Observation Network of China and 87 radiosonde stations are selected to validate the proposed CHZ model, and hourly ZTD data derived from GNSS are used to establish the CHZ model. Statistical result shows that the averaged root mean square and Bias of the CHZ model are 21.12 and −2.51 mm, respectively, in the whole of China. In addition, the application of CHZ model in precision point positioning (PPP) show that the convergence time is improved by 34%, 15%, and 35%, respectively, in N, E, and U components when compared to GPT3-based PPP.

Index Terms—Global navigation satellite system, high-precision ZTD model, large height difference, zenith tropospheric delay.

I. INTRODUCTION

THE wireless electromagnetic wave signal will be refracted and bent when it passes through the troposphere due to the atmospheric refraction effect, which is called tropospheric delay

Qingzhi Zhao, Jing Su, Xiaoya Zhang, and Jifeng Wu are with the Xi'an University of Science and Technology, Xi'an 710000, China (e-mail: zhaoqingzhia@163.com; jingsu0806@163.com; 21210226082@stu.xust.edu.cn; wujifeng@xust.edu.cn).

Chaoqian Xu and Yibin Yao are with the Wuhan University, Wuhan 430000, China (e-mail: cqxu@whu.edu.cn; ybyao@whu.edu.cn).

[1]. The projection of tropospheric delay into the zenith direction is called zenith tropospheric delay (ZTD), which is one of the main error sources in space geodesy [2]. Therefore, establishing a high-precision ZTD model is of considerable importance for space geodesy techniques, such as global navigation satellite system (GNSS) and very long baseline interferometry [3].

Empirical ZTD models can be divided into two types: tropospheric delay models based on meteorological parameters and nonmeteorological parameters. The models of Saastamoinen, Hopfield, and Black typically use the observed meteorological parameters [4], [5], [6]. The Hopfield model is first established using the global meteorological data of 18 stations and then improved by adding the temperature gradient [5]. The Saastamoinen model divides the troposphere into two sections according to the variation law of temperature with elevation during atmospheric temperature calculation, which improves the accuracy of troposphere delay calculation results to a certain extent [4]. The Black model is improved by the Hopfield model and calibrated the influence of atmospheric refraction on signal propagation path bending [7]. The accuracy of the abovementioned ZTD models based on meteorological parameters are similar, and small differences are observed under different conditions. The estimated ZTD precision varies from decimeter to centimeter under various conditions [8]. However, the abovementioned ZTD model based on meteorological parameters is excessively dependent on the observed data, which cannot be used for those regions without meteorological parameters. Therefore, establishing a high-precision ZTD model without nonmeteorological parameters gradually becomes the focus.

The typical ZTD models, such as the series models of the University of New Brunswick (UNB), the European Geostationary Navigation Overlay Service (EGNOS), Tropospheric Grid (TropGrid), and Global Pressure and Temperature (GPT), have been established using the historical meteorological data or numerical weather prediction (NWP) products and widely used on regional or global scales. The UNB series model grids the standard atmospheric parameters in the United States at an interval of 15° in the latitudinal direction and calculates the required meteorological data, such as temperature, pressure, and water vapor pressure [9], [10], [11]. The accuracy of the UNB model in North America can reach 2 cm, but the correction accuracy of the model on a global scale is equivalent to that of the Saastamoinen model [12]. The EGNOS model is then established by the simplified UNB3 model and improved by the method of estimating meteorological parameters by [13], and the accuracy of the EGNOS model can reach 3 cm on a global scale.

The grid-based ZTD models have been gradually developed with the development of NWP. The TropGrid model is initially proposed, and the meteorological parameters of the model are stored in the grid database [14]. The global average accuracy of the TropGrid model is approximately 3.8 cm, which is considerably improved compared with the UNB3 model [14]. The advanced version of TropGrid (TropGrid2) is then developed, which is slightly better than the previous one on a global scale [15]. In addition, the GPT series models, such as GPT [16], GPT2 [17], GPT2w [18], and GPT 3 [19], have been gradually developed. Compared with the previous version, the GPT3 model further optimized the gradient model grid, and the averaged root mean square (RMS) and Bias reached 4.7 and −0.99 cm, respectively, in the United Kingdom [3]. Li et al. [20] established a nonmeteorological ZTD model based on empirical vertical reduction functions, namely IGGtrop_SH and IGGtrop_rH. The IGGtrop_SH model considers the changes in annual and semiannual periods of ZTD, while the IGGtrop_rH model only considers the annual period. In addition to the above models, other models, such as the Global Zenith Tropospheric Delay (GZTD) [2], [8], Global Tropospheric Model (GTrop) [21], Global Hopfield (GHop) model [22], and Africa Tropospheric (AFRC-Trop) model [23] have been proposed and validated on regional or global scales with fluctuating accuracies between 3.5 to 4.2 cm.

With the encryption of GNSS observation stations on a global scale, some empirical ZTD models were also established using the GNSS-derived ZTD. Compared with NWP products, the GNSS-derived ZTD has high accuracy with an RMS of approximately 4 mm [24]. Therefore, previous studies have focused on establishing the ZTD model using high-precision ZTD time series derived from GNSS observations. The SHanghai Astronomical observatory tropospheric delay model (SHATrop) is established in China using GNSS-derived ZTD of 223 stations from the Crustal Movement Observation Network of China (CMONOC) over the period of 2016 to 2017 [25]. In the next year, [25] improved the SHATrop model using the GNSS data of 310 stations derived from CMONOC and the International GNSS Service over the period of 2012 to 2018, and this model considers the exponential and periodic functions as well as the seasonal changes in ZTD, which is called the SHATrop-Extend (SHATropE) model. The averaged RMS of the SHATropE model in China is approximately 3.5 cm. Huang et al. [26] developed a ZTD vertical stratification model considering spatiotemporal factors based on the second Modern-Era Retrospective analysis for Research and Applications (MERRA-2) data, which is named the GZTD-H model. compared to model GPT2w, the model GZTD-H also attains improvements of 11% over the precise ZTD products acquired at IGS sites.

Numerous empirical ZTD models have been established using meteorological, NWP, or GNSS data, and the general accuracy of a typical ZTD model is acceptable on regional or global scales; however, the performance of previous ZTD models in regions with a large height differences is hardly investigated [2], [19]. In addition, some models, such as GZTD [2], IGGtrop_SH [21] and GZTD-H [26], have considered the height influence on ZTD. However, more refined height relationships for empirical ZTD model should be further considered for regional ZTD models

with large height differences. Obtaining high-precision ZTD initial values is necessary for GNSS high-precision data processing, and the abovementioned empirical ZTD models encounter difficulties in meeting the requirement in regions with large height differences. Therefore, establishing a high-precision ZTD model for regions with large height differences is of considerable practical significance.

The GPT3 model is an empirical model of global pressure and temperature based on the monthly mean pressure stratification data of the European weather forecasting center. This model improves the mapping function coefficient, thus, effectively overcoming the mapping function error caused by low-altitude cutoff angles. A previous study proved that a significant correlation existed between ZTD and height. Therefore, the relationship between height and residuals of GPT3 and GNSS-derived ZTD are investigated, and a high-precision ZTD model of altitude-related correction for China (CHZ) based on the GPT3 model is developed. The initial ZTD value of the CHZ model is first calculated by the GPT3 model. In addition, this model considers the influence of the periodic terms of ZTD residuals and the height influence on ZTD periodic residuals. China is selected to validate the performance of the CHZ model due to its large height difference, and four subregions have been divided. Statistical results show the good performance and robustness of the proposed CHZ model, especially for the Qinghai–Tibet with a largest height difference in China. Comparison results with the previous studies also indicate the superiority of the proposed CHZ model in China.

II. STUDY AREA AND DATA DESCRIPTION

A. Study Area

China is located in the middle latitudes of the northern hemisphere in the southern part of Eurasia (18°N–54°, 73°E–135°E), with a vast territory and a large north-south span. The terrain is high in the west and low in the east, which is distributed in a ladder-like manner. The first step of the terrain is southwest China, with an average altitude of more than 4500 m. The second step is central China, which has an average altitude of 1000–2000 m. The third step is eastern China, with an altitude of more than 500 m [27], [28]. In addition, China has a typical continental monsoon climate, with distinct dry and wet seasons and four diverse seasons. The climate of different regions also remarkably varies [29], [30]. Affected by topography and climate, GNSS stations are distributed more in the east and less in the west, with dense stations in North and South of China and sparse stations in Qinghai–Tibet Plateau and Northwest of China. Therefore, the distance between GNSS stations is larger in Qinghai–Tibet Plateau and Northwest of China than that in South and North of China. A previous study also showed that ZTD is substantially affected by height and climate [31], [32]. Therefore, China is an ideal region for the experiment as determined in this article.

B. GNSS-Derived ZTD

The GNSS observation is obtained from the Crustal Movement Observation Network of China (CMONOC). CMONOC
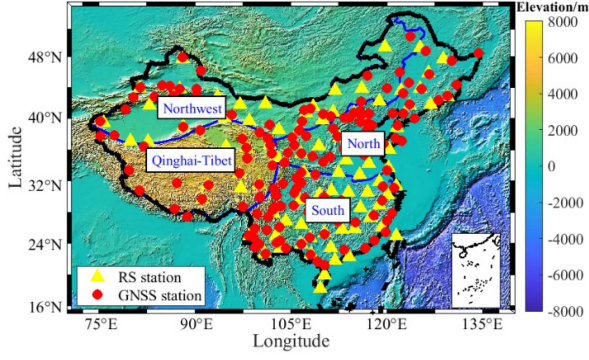
Fig. 1. Geographical distributions of selected GNSS and RS stations and four subregions divided in China.

was established from 1997 to 2000 and was officially put into operation in 2011. It has been built with more than 264 GNSS continuous stations and approximately 2000 discontinuous stations, including 27 network engineering reference stations. These stations have high precision and good stability and can provide high-precision observation data for GNSS meteorology and other studies [33], [34], [35]. A total of 164 out of 264 GNSS stations have been selected due to the complete observation data over the experimental period and the uniform distribution in China. GNSS observations are processed by the precision point positioning (PPP) technique, and the corresponding processing configurations can be referred to our previous work [36]. Finally, the GNSS-derived ZTD of 164 GNSS stations is obtained with a time resolution of 1 h. Different climates have varying impacts on the periods of ZTD [32]; therefore, China is divided into four regions according to the climate characteristics: Northwest, North, South, and Qinghai–Tibet [37]. Fig. 1 presents the geographical distributions of GNSS and radiosonde (RS) stations and the subregions divided in China.

C. ZTD Derived From GPT3

GPT series models, which include GPT, GPT2, GPT2w, and GPT 3, are the tropospheric empirical correction models with the widest application and the highest accuracy worldwide. The first three models have been extensively described and investigated previously [17], [18], [19]. The GPT3 model is an empirical model of global pressure and temperature based on the monthly mean pressure stratification data of the European mesoscale weather forecasting center [20]. Similar to the GPT2w model, the GPT3 model uses geophysical model functions as the mapping function. This model improves the mapping function coefficients, effectively overcomes the mapping function errors caused by low-altitude cutoff angles, and adds the following two parameters: atmospheric weighted average temperature and water vapor pressure decline rate [38]. The input parameters of the GPT3 model include station location information (longitude, latitude, and elevation) and time information (day of year, doy), and the output parameters are pressure, temperature, water vapor pressure, and its decline rate, mapping function coefficient and other information. The parameter grid file of the GPT3 model includes the spatial resolution of $1° \times 1°$ and $5° \times 5°$,

respectively. In this article, the parameter grid file with a spatial resolution of $1° \times 1°$ is selected to calculate the estimated ZTD, and the specific procedures for calculating ZTD based on the GPT3 model are as follows.

1) Determining the corresponding meteorological parameters of four grid points surrounding the target point inputted using the GPT3 model.
2) Calculating the corresponding values of four grid points for the target point height based on the following formulas:

$$P = P_0 \cdot e^{\frac{g_m \cdot dM}{R_g \cdot T_v}(h-h_0)}$$

$$T_v = T_0(1 + 0.6077 \cdot Q)$$

$$T = T_0 + dT^* dh$$

$$e_0 = Q^* P_0/(0.622 + 0.378^* Q)/100$$

$$e = e_0(P^* 100/P_0)^{\lambda+1} \quad (1)$$

where P_0, T_0, and e_0 are the pressure (hPa), temperature (K), and water vapor pressure (mbar) of each grid point, respectively; P, T, and e are the pressure, temperature, and water vapor pressure at the target point, respectively; g_m is the gravity with the value of 9.80665 m/s²; dM is the molar mass of dry air, and the value is 28.965×10^{-3} kg/mol; R_g is the general gas constant with the value of 8.3143 J/K/mol, and T_v is the virtual temperature (Kelvin); Q is the specific humidity, dT is the temperature lapse rate, λ is the water vapor decrease coefficient; h and h_0 are the heights of station and grid point, respectively.

3) Obtaining the pressure, temperature, and water vapor pressure of target points using the corresponding parameters of four nearby grid points by using bilinear interpolation.
4) Calculating zenith hydrological delay (ZHD). ZHD can be calculated by the empirical formula and expressed as follows:

$$ZHD = \frac{0.0022768 \cdot P}{1 - 0.00266 \cdot \cos 2\phi - 0.00028 \cdot h} \quad (2)$$

where P is the surface pressure, ϕ is the latitude, and h is the geoid height of the station.

5) Calculating zenith wet delay (ZWD). ZWD is also calculated on the basis of the empirical formula proposed by [38]:

$$ZWD = 10^{-6}(k_2' + \frac{k_3}{T_m})\frac{R_d}{(\lambda+1)g_m}e_s$$

$$k_2' = k_2 - k_1 M_w/M_d$$

$$R_d = R/M_d \quad (3)$$

where R is the molar gas constant, and the value is 8.314 J/(mol·k); M_w and M_d are the molar mass of water and dry air with values of 18.0512 kg/mol and 28.965×10^{-3} kg/mol, respectively; k_1, k_2, and k_3 are constants with values of 77.604 ± 0.014 k/mbar, 64.79 ± 0.08 k/mbar, and $(3.776 \pm 0.04) \times 10^5 k^2$/mbar, respectively; R_d represents the gas constant of the dry component, g_m is the gravitational acceleration at the mass center of the vertical column of the atmosphere with a value of 9.80655 m/s², and T_m is the weighted average temperature.

6) After the ZHD and ZWD are calculated, the final ZTD can be obtained by combining ZHD and ZWD

$$ZTD = ZWD + ZHD. \qquad (4)$$

D. ZTD Derived From RS Data

The meteorological data, such as temperature, pressure, humidity, and wind speed at different altitudes from ground to approximately 30 km, are detected by releasing the sounding balloon made of natural latex through the sensor installed on the sounding balloon, and these observation data are then transmitted to the ground observation station [39]. These data are a set of high-quality RS station datasets with the highest spatial–temporal density and the most complete data in the world at present. In addition, they also have high vertical resolution and accuracy [40]. Therefore, RS data are often used as the truth value to evaluate the accuracy of meteorological elements obtained by other methods. Integrated Global Radiosonde Archive version 1 (IGRA1) started in the 1960s and created RS data from the National Climatic Data Center (NCDC) of the United States. IGRA1 provides meteorological parameters, such as ground temperature, pressure, and water vapor pressure, to the height of approximately 30 km at more than 1500 stations worldwide. Haase et al. [41] used GPS-derived ZTD to evaluate the accuracy of IGRA-derived ZTD and found that the standard deviation (STD) between IGRA and GPS was 12 mm, which demonstrated a good accuracy. In August 2016, NCDC released the second generation of IGRA (IGRA2), which is superior to IGRA1 considering the number of stations, observation length, and data collection sources [39].

The ZTD can be calculated using the RS data and the following presents the specific steps.

1) Calculating ZWD as follows:

$$ZWD = 373000 \cdot \sum \left(e_i / T_i^2 \right) \cdot \Delta h_i \qquad (5)$$

where Δh_i is the height of each layer, and e_i is the water vapor pressure (mbar) at the ith layer.

2) The ZHD is further calculated by integral.

$$ZHD = 77.6 \cdot \sum \left(P_i / T_i \right) \cdot \Delta h_i. \qquad (6)$$

Finally, the ZTD can be obtained using (4) by combining ZWD and ZHD. In this article, 87 RS station have been selected over the period of 2012 to 2018 in China, and Fig. 1 also gives the geographical distribution of RS used in this article.

III. HIGH-PRECISION CHZ

A. Validation of GNSS-Derived ZTD

A total of 28 collocated stations between GNSS and RS over the period of 2012 to 2018 are determined for the experiment to validate the precision of GNSS-derived ZTD using the PPP technique. The collocated principle is that the horizontal and vertical distances between GNSS and RS are less than 30 km and 500 m, respectively [35]. An empirical height correction model is also performed in accordance with [42] to further reduce the influence of height on the comparison of ZTD between GNSS
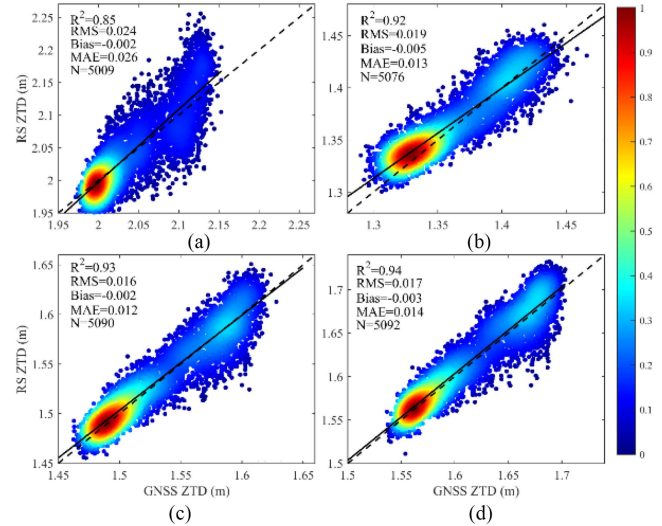

Fig. 2. Scatter probability density plots of ZTD comparisons derived from GNSS and RS at GSPL, HECC, QHYS, and SCGZ stations over the period of 2012 to 2018.

TABLE I
STATISTICAL RESULTS OF AVERAGE RMS, BIAS, AND MAE BETWEEN GNSS-
AND IGRA2-DERIVED ZTD OVER THE PERIOD OF 2012 TO 2018 (UNIT: M)

Regions	averaged height difference	RMS	Bias	MAE
North	327.4	0.023	-0.011	0.024
South	127.5	0.017	-0.003	0.014
Qinghai-Tibet	99.4	0.016	-0.004	0.012
China	185.4	0.019	-0.002	0.018

and RS. From 28 collocated stations, 4 stations (GSPL, XZNQ, QHYS, and SCGZ) evenly distributed in four subregions of China are selected. Fig. 2 shows the scatter density diagram of ZTD at UTC 00:00 and 12:00 derived from the four collocated stations over the period of 2012 to 2018. It can be observed that the GNSS-derived ZTD has a good consistency with that from RS at four selected stations, and the correlation coefficients are 0.85, 0.91, 0.93, and 0.94, respectively (P < 0.05). In addition, the RMS, Bias and mean absolute error (MAE) at the four stations are 0.034/−0.012/0.026 m, 0.016/−0.005/0.013 m, 0.016/−0.002/0.012 m, and 0.017/−0.003/0.014 m, respectively. The comparison of ZTD at 28 collocated stations over the period of 2012 to 2018 is performed to further analyze the performance of GNSS-derived ZTD in the whole of China, and Table I gives the statistical result of ZTD differences between GNSS and RS in the four subregions of China. The statistical results show that the averaged RMS, Bias, and MAE of GNSS-derived ZTD in China are 0.023, 0.017, −0.012, and 0.015 m, respectively, which verifies the good performance of ZTD used in this article. In addition, the average height difference between GNSS and RS stations is the largest in North China, the
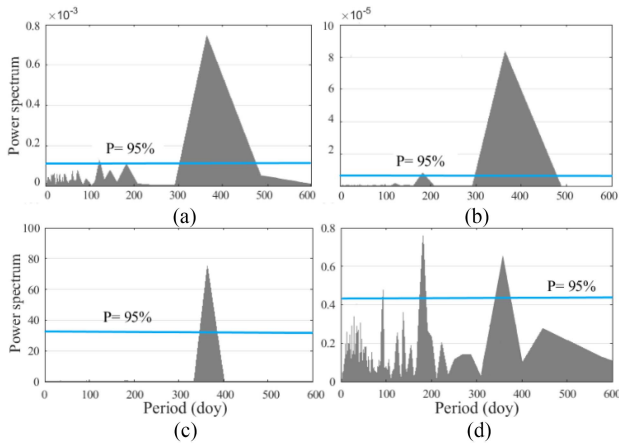
Fig. 3. Lomb–Scargle periodograms of four selected stations (HECC, GSPL, QHYS, and SCGZ) distributed in four subregions of China over the period of 2012 to 2018.

Northwest is second, and Qinghai–Tibet is the smallest, which corresponds to the largest RMS in North and the smallest RMS in Qinghai–Tibet. Therefore, the RMS value is generally decreased with the reduction in average height difference between GNSS and RS stations.

B. Periodic Analysis of ZTD Residuals

A previous study proved that the ZTD is affected by latitude and seasons [26]. Therefore, the ZTD residuals between the GPT3 model and GNSS at 164 GNSS stations are further analyzed to determine the specific periodical terms of ZTD in each subregion of China. Herein, the Lomb–Scargle periodogram (LSP) method is introduced because it has no equispaced time series requirement and it can effectively reflect the real characteristics of time series and calculate the hidden time signals [43]. The specific periodical terms of ZTD residual at each GNSS station are first determined, and Fig. 3 presents the LS diagram of the four selected stations (HECC, GSPL, QHYS, and SCGZ) distributed in four subregions of China. It can be observed that the specific periodical signals can be determined for the four selected stations by using the LSP method. After the periodical signal of ZTD residual at each GNSS station is determined, the main periodical terms of each subregion in China are obtained by selecting the existing periodical term in 75% of the total number of GNSS stations. Finally, the specific periodical terms of each subregion are obtained and used for fitting the ZTD periodic residual of each subregion in China. Table II shows the determined periodical signals of ZTD residual in four subregions, wherein the main period in Qinghai–Tibet is annual. Annual and semiannual periods existed in Northwest China, while the annual and seasonal (120) periods emerged in North China. For the South region, annual, semiannual and seasonal (120) are determined by the LSP method. These results prove the necessity of dividing China into different climatic regions, and the ZTD residual should be fitted using various periodical models in China.

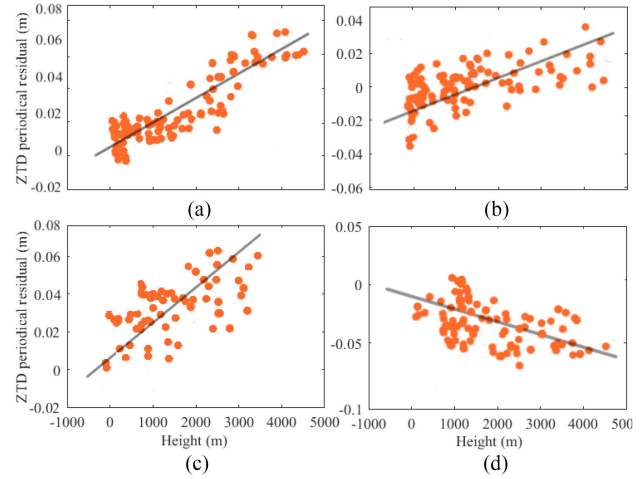| Regions	Period	Percentage
Qinghai-Tibet	annual	81.8% (18/22)
Northwest	Annual and semi-annual	77.4% (24/31)
North	Annual and season (120)	78.0% (39/50)
South	Annual, semi-annual and season (120)	78.7% (48/61)

Fig. 4. Distributions of annual average ZTD periodical residual and height in four regions of China over the period of 2012 to 2018.

C. Relationship Analysis Between ZTD Periodical Residual and Height

In addition to the periodic factor, the ZTD value is also affected by the height. Although the height factor has been considered by the GPT3 model when calculating the corresponding P and T at GNSS stations [19], the height-related residual still existed for regions, especially in China with large height differences. Similarly, the developed ZTD models without considering the height factor, such as the ISAAS model [44], the GHOP model [22], and the AFRC-TROP model [23], are significantly affected by height. Therefore, the relationship between ZTD periodical residual and height is further explored in this section. Four periodical models of ZTD residual are established in accordance with the periodical signals of ZTD determined above in each subregion of China. Therefore, the averaged ZTD periodical residual between ZTD residual and four established periodical models of ZTD residual is obtained at 164 GNSS stations over the period of 2012 to 2018. Fig. 4 shows the scatter plot between height and ZTD periodical residual of 164 GNSS stations in four subregions of China. It can be observed that an evident linear relationship existed between ZTD periodical residual and height, and the correlation coefficients are 0.78,
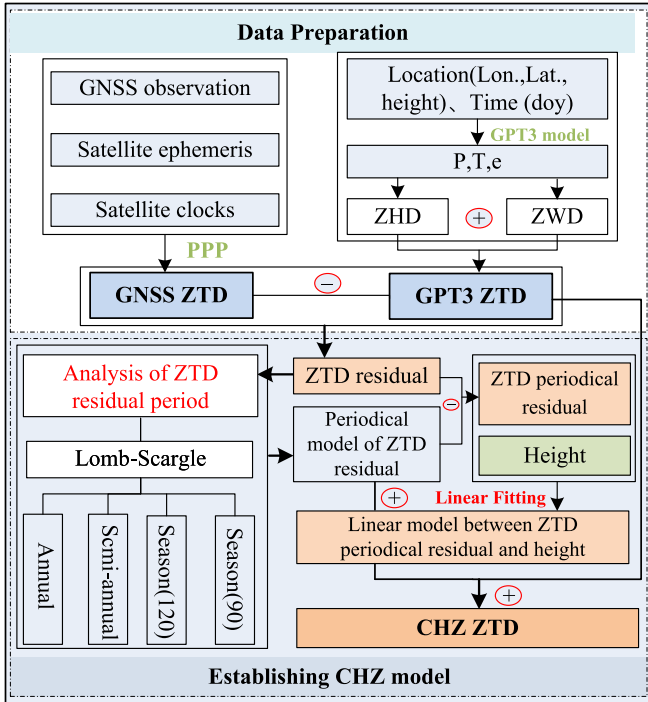
Fig. 5.   Overall flow chart of establishing the CHZ model.

Fig. 6.   Relationship between internal (STD) and external (RMS) accuracies of CHZ model and height over the period of 2012 to 2018.

0.82, 0.79, and 0.71, respectively, for the four subregions of China (Q < 0.05). In addition, a large height difference indicates an evident linear relationship. However, a negative relationship existed between ZTD periodical residual and height in South China, while a positive relationship is evident in its three other regions. Such a finding further verifies the necessity of dividing China into different climate regions. Therefore, geographical location and height factors must be considered for establishing high-precision ZTD models in regions with large height differences.

D. High-Precision ZTD Model for China (CHZ model)

Different periods of ZTD residual between GNSS and GPT3 models and various linear relationships between ZTD periodical residual and height both existed in the four subregions of China. Therefore, a further altitude-related correction of the residuals between GPT3 and GNSS-derived ZTD is performed to build a more sophisticated ZTD model in China to further improve the accuracy of estimated ZTD, which is called the high-precision CHZ. Fig. 5 shows the overall flow chart of establishing the CHZ model, which considers the influences of periodic, height and climate on ZTD.

The specific procedures for establishing the CHZ model can be summarized as follows.
1) Estimating hourly ZTD using the PPP technique at 164 GNSS stations over the period of 2012 to 2018.
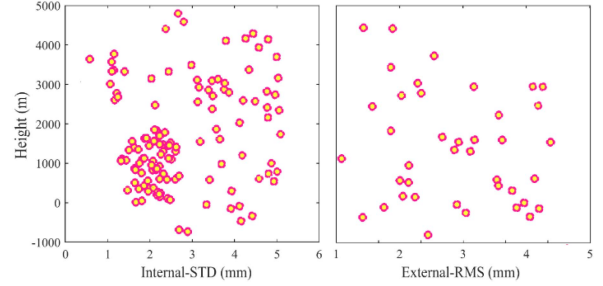2) Calculating hourly ZTD values at GNSS stations based on the GPT3 model.

3) Obtaining the residual between GNSS- and GPT3-derived ZTD at 164 stations

$$d_{\text{res}} = \text{ZTD}_{\text{GNSS}} - \text{ZTD}_{\text{GPT3}} \qquad (7)$$

where d_{res} is the ZTD residual between the GNSS and GPT3 models; ZTD_{GNSS} and ZTD_{GPT3} are GNSS- and GPT3-derived ZTD, respectively.

4) Determining the specific periodical signals of ZTD residual at each region of China and establishing the periodical models of ZTD residual. Previous analysis in Section III-B has determined the specific periodical signals for each region. Therefore, the general periodical model can be expressed as

$$
\begin{aligned}
d_{\text{res}}^{\text{range}} &= A_0^{\text{range}} + A_1^{\text{range}} \cos(\tfrac{\text{doy}}{365.25}2\pi - \phi_1^{\text{range}}) + \dots \\
&\quad A_2^{\text{range}} \cos(\tfrac{\text{doy}}{365.25}4\pi - \phi_2^{\text{range}}) + \dots \\
&\quad A_3^{\text{range}} \cos(\tfrac{\text{doy}}{365.25}6\pi - \phi_3^{\text{range}}) + \dots \\
&\quad A_4^{\text{range}} \cos(\tfrac{\text{doy}}{365.25}8\pi - \phi_4^{\text{range}}) \\
d_{\text{res+per}}^{\text{arb}}(i) &= a^{\text{range}}(i) * h + b^{\text{range}}(i)
\end{aligned}
\qquad (8)
$$

where $d_{\text{model\_res}}^{\text{range}}$ is the periodical model of ZTD residual; $A_1^{\text{range}} - A_4^{\text{range}}$ are the coefficients of annual, semiannual, and seasonal (120) and (90) periods, respectively; and $\phi_1^{\text{range}} - \phi_1^{\text{range}}$ are the amplitudes of annual, semiannual and seasonal (120) and (90) periods, respectively. doy is the day of year while range represents the climate subregions of China, which are Northwest, North, South, and Qinghai–Tibet, respectively.

5) Obtaining the ZTD periodical residual between ZTD residual and periodical model of ZTD residual

$$d_{\text{res+per}}^{\text{range}}(i) = d_{\text{res}}^{\text{range}}(i) - d_{\text{model\_res}}^{\text{range}}(i) \qquad (9)$$

where $d_{\text{res+per}}^{\text{range}}$ is the ZTD periodical residual, and i is the corresponding epoch.

6) Establishing a linear relationship between ZTD periodic residual and height in each region of China. Section III-C shows a linear relationship existing between ZTD periodic residual and height. Therefore, the corresponding relationship in each region can be expressed as follows:

$$d_{\text{res+per}}^{\text{arb}}(i) = a^{\text{range}}(i) * h + b^{\text{range}}(i) \qquad (10)$$

where a^i and b^i are the slope and intercept of linear equations, respectively.
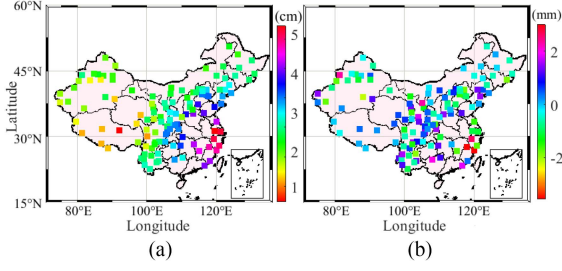
Fig. 7. Distribution of RMS and Bias of GNSS- and CHZ- ZTD for internal validation over the period of 2012 to 2018.

Fig. 8. Time series of CHZ- and GNSS-derived ZTD at XZLL, QHBC, XZDX, and HEYY stations over the period of 2012 to 2018.

7) Calculating the ZTD and ZTD periodical residuals based on (8) and (10), respectively, at arbitrary location and height

$$
\begin{aligned}
d_{res}^{arb} = A_0^{range} + A_1^{range} \cos(\frac{doy}{365.25} 2\pi - \phi_1^{range}) + \ldots \\
A_2^{range} \cos(\frac{doy}{365.25} 4\pi - \phi_2^{range}) + \ldots \\
A_3^{range} \cos(\frac{doy}{365.25} 6\pi - \phi_3^{range}) + \ldots \\
A_4^{range} \cos(\frac{doy}{365.25} 8\pi - \phi_4^{range})
\end{aligned}
\tag{11}
$$

$$
d_{res+per}^{arb}(i) = a^{range}(i) * h + b^{range}(i) \tag{12}
$$

where d_{res}^{arb} and $d_{res+per}^{arb}$ are the ZTD and ZTD periodical residuals calculated at arbitrary location and height, respectively.

8) Therefore, the CHZ-derived ZTD can be obtained by adding the ZTD and ZTD periodical residuals to GPT3-derived ZTD

$$
ZTD_{CHZ}^{arb}(i) = GPT3_{GPT3}^{arb}(i) + d_{res}^{arb}(i) + d_{res+per}^{arb}(i) \tag{13}
$$

where ZTD_{CHZ}^{arb} is the CHZ-derived ZTD.

IV. ANALYSIS AND EVALUATION OF THE CHZ MODEL

A. Relationship Between CHZ-Derived ZTD and Height

The CHZ model proposed in this article considers the impact of height on ZTD; therefore, the relationship between CHZ-derived ZTD and height is first analyzed. The randomly selected hourly ZTD data of 123 GNSS stations over the period of 2012 to 2018 in China are used to establish the CHZ model, and the corresponding data of 41 other GNSS stations are utilized for external validation. Fig. 7 shows the STD and RMS of ZTD difference between CHZ and 123/41 GNSS stations, respectively over the period of 2012 to 2018. It can be found that there is no evident linear relationship existed between CHZ-derived ZTD and height for STD and RMS. This finding verifies that the proposed CHZ model effectively overcomes the influence of the height factor on ZTD and is suitable for ZTD estimation in regions with large height differences.

B. Internal Validation of the CHZ Model

The internal accuracy of the proposed CHZ model is validated to evaluate its performance. The STD, Bias, and MAE of ZTD differences between the CHZ model and GNSS stations are calculated over the period of 2012 to 2018. Fig. 7 shows the
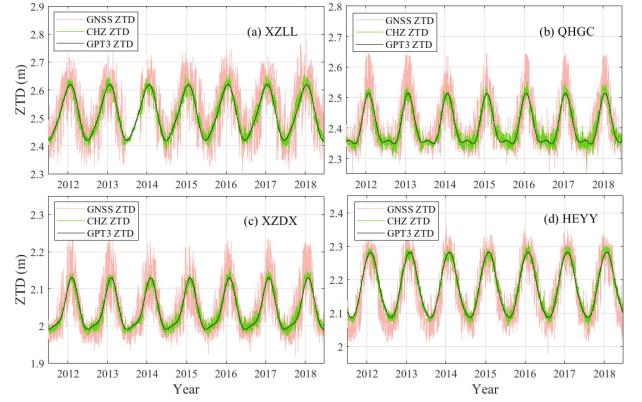
STD and Bias distributions of the CHZ model at 123 GNSS stations in China. It can be found that STD values are relatively small in Northwest and Qinghai–Tibet of China, which is mainly due to the height factor considered by the CHZ model and the relatively low ZTD values in those regions. In addition, the values of STDs are relatively large in South China. This finding is mainly due to the existing large atmospheric water vapor content and the remarkable changes in the South of China, which cannot be precisely modeled [45]. Table III presents the statistical result of STD, Bias, and MAE for the CHZ model at four regions in each season over the period of 2012 to 2018. The averaged STD, Bias, and MAE of the CHZ model in four regions are 19.0/24.5/23.8/17.8 mm, 1.7/2.7/2.9/1.3 mm, and 23.1/25.3/24.3/18.2 mm, respectively. Such results verify the good internal accuracy of the proposed CHZ model established in this article. In addition, the STD is the largest in summer and the smallest in winter in four regions of China, which is due to the large ZTD value and relatively violent water vapor fluctuation in summer [46].

C. External Validation of the CHZ Model

The performance of the proposed CHZ model is further evaluated using the other 43 GNSS stations, which are not used for establishing the CHZ model. In addition, the corresponding ZTD values at UTC 00:00 and 12:00 derived from the 87 RS stations over the period of 2012 to 2018 are also used to validate the proposed CHZ model in this section.

1) Comparison With GNSS-Derived ZTD: The CHZ-derived ZTD at 43 GNSS stations with a time resolution of 1 h is first calculated over the period of 2012 to 2018 and compared with that from GNSS observation. Fig. 8 shows the ZTD time series derived from GNSS, GPT3, and CHZ models at four stations (XZLL, QHBC, XZDX, and HEYY) distributed in four regions of China over the period of 2012 to 2018. It can be observed that CHZ-derived ZTD has a good consistency with that from GNSS, while only the periodical changes in ZTD can be presented by the GPT3 model at four selected stations. This finding is due to the height and periodical signals of ZTD residual, which are also considered by the CHZ model. Therefore, more sophisticated

TABLE III
STATISTICAL RESULT OF AVERAGED STD, BIAS, AND MAE OF THE CHZ MODEL FOR INTERNAL VALIDATION AT FOUR SEASONS IN FOUR REGIONS OF CHINA
OVER THE PERIOD OF 2012 TO 2018 (UNIT: MM)

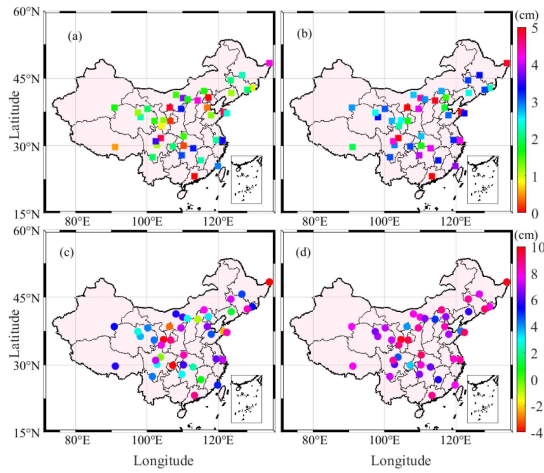| Region	Index	Spr.	Sum.	Aut.	Win.	Aver.
Northwest	STD	18.9	20.1	18.0	15. 5	19.0
	Bias	-1.8	-2.4	-2.1	-1.3	-1.9
	MAE	17.9	22.1	19.2	16.3	17.8
South	STD	24.6	27.6	24.2	21.7	24.5
	Bias	-2.9	-3.6	-2.9	-2.9	-3.1
	MAE	26.1	29.0	22.4	22.1	24.9
North	STD	23.9	26.9	24.6	19.8	23.8
	Bias	-1.7	-3.9	-3.2	-2.3	-2.8
	MAE	21.3	30.1	26.1	22.7	25.1
Qinghai-Tibet	STD	17.8	23.4	16.3	13.6	17.8
	Bias	-1.2	-2.7	-1.2	-0.9	-1.5
	MAE	21.2	22.3	16.9	16,3	20.1

Fig. 9. Distributions of RMS and Bias of GNSS-, CHZ-, and GPT3-derived ZTD for external validation at 43 GNSS stations over the period of 2012 to 2018.

Fig. 10. Time series of CHZ- and RS-derived ZTD at four stations over the period of 2012 to 2018.

changes in ZTD can be modeled. Fig. 9 provides the RMS and Bias distributions of ZTD differences between GNSS and GPT3/CHZ models at 41 stations over the period of 2012 to 2018 to further evaluate the performance of the CHZ model over the whole of China. It can be found that the RMS and absolute Bias of the CHZ model are smaller than that of the GPT3 model, which verifies the superiority of the proposed CHZ model. In addition, the performance of the CHZ model is effective in Northwest and Qinghai–Tibet of China, which is consistent with the internal validation of the CHZ model. Table IV presents the statistical result of RMS and Bias of GPT3 and CHZ models in four subregions of China over the period of 2012 to 2018. The results indicate that the CHZ model is superior to the GPT3 model in four subregions of China, and the average improvement rate reaches 16.45%. In addition, the Bias of the CHZ model is largely reduced in Qinghai–Tibet with values of 3.88 mm compared with that of the GPT3 model because the ZTD residual affected by the height has been considered by the CHZ model. The averaged RMS, Bias, and MAE of
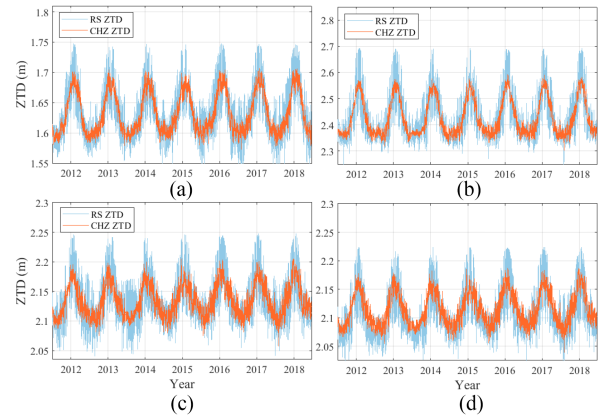
GPT3 and CHZ models are 25.3/21.1 mm, −4.8/−2.5 mm, and 26.1/23.5 mm. These results verify the good performance and reliability of the proposed CHZ model in this article.

2) Comparison With RS-Derived ZTD: RS-derived ZTD data over the period of 2012 to 2018 at 00:00 and 12:00 UTC of 87 stations is selected to verify the performance of the CHZ model, and the RMS, Bias, and MAE between the RS and CHZ modle are calculated. Fig. 10 shows the time series comparison of CHZ- and RS-derived ZTD at four RS stations (CHM00051463, CHM00053915, CHM00053772, and CHM00056571) distributed in four subregions of China over the period of 2012 to 2018. Fig. 10 shows that the CHZ-derived ZTD has good consistency with that from RS. Fig. 11 also shows the average RMS, Bias, and MAE of the ZTD residuals between the CHZ model and RS at 87 RS stations in four subregions over the period of 2012 to 2018. The statistical results show that the average RMS, Bias, and MAE between the CHZ model and RS are 27.0, 5.1, and 29.3 mm, respectively. In addition, it also can be observed that a good performance of the CHZ model is obtained in the Qinghai–Tibet region of China. This result

TABLE IV
STATISTICAL RESULT OF AVERAGED RMS, BIAS, AND MAE FOR GPT AND CHZ MODELS IN FOUR REGIONS OF CHINA OVER THE PERIOD OF 2012 TO 2018
(UNIT: MM)

Region	RMS		Bias		MAE	
	GPT3	CHZ	GPT3	CHZ	GPT3	CHZ
Northwest	24.8	19.0	-6.1	-3.5	25.3	23.1
South	28.5	24.2	-3.7	-3.1	27.9	24.4
North	25.6	23.1	-4.2	-1.8	26.1	22.7
Qinghai-Tibet	22.2	18.1	-5.4	-1.8	24.9	23.6
Aver.	25.3	21.1	-4.8	-2.5	26.1	23.5

TABLE V
STATISTICAL RESULT OF AVERAGED RMS FOR CHZ, IGP2W, AND GTROP MODELS AT FOUR SEASONS IN DIFFERENT REGIONS OF CHINA OVER THE PERIOD OF
2012 TO 2018 (UNIT: MM)

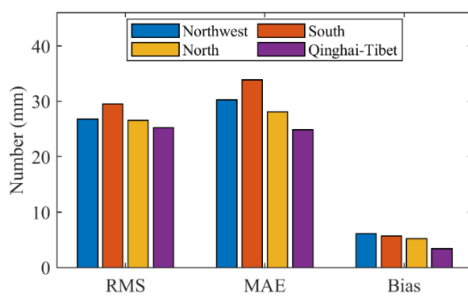| region	model	Spr.	Sum.	Aut.	Win.	Aver.
North	IGPT2w	29.9	27.0	23.7	26.4	26.8
	Gtrop	28.5	24.5	23.1	24.5	25.2
	CHZ	25.4	22.3	21.6	22.7	23.3
South	IGPT2w	29.7	32.6	27.8	26.5	29.1
	Gtrop	27.9	29.6	26.5	24.1	27.0
	CHZ	24.6	27.6	24.2	21.7	24.5
Qinghai-Tibet	IGPT2w	24.9	28.9	25.0	23.7	23.1
	Gtrop	21.8	25.5	23.5	22.1	21.7
	CHZ	17.8	22.4	19.3	19.6	18.3
Northwest	IGPT2w	25.3	27.6	26.0	23.9	25.7
	Gtrop	23.2	25.7	23.3	22.5	23.7
	CHZ	20.9	22.1	22.0	20.6	21.4

Fig. 11. Statistical result of RMS, Bias, and MAE between CHZ and RS-derived ZTD in four regions of China over the period of 2012 to 2018.

further verifies the effectiveness and applicability of the CHZ model proposed in this article for regions with large elevation differences.

D. Comparison With the Previous Models

Two typical ZTD models, namely the GTrop model [21] and the improved IGPT2w model [47], are selected and compared with the CHZ model in China to further verify the performance

of the proposed CHZ model. The hourly ZTD of 164 GNSS stations over the period of 2012 to 2018 is used to establish the GTrop, IGPT2w, and CHZ models in each region of China. Table V gives the statistical results of averaged STDs of three models over the period of 2012 to 2018. It can be found that the CHZ model is superior to the two other models in four subregions of China at different seasons, and the largest improvement occurred at the Qinghai–Tibet with average improvement rates of 15.7% and 20.8, respectively, when compared with GPT2w and GTrop models. The averaged STD, Bias, and MAE of IGPT2w, GTrop, and CHZ models are 26.38/24.47/21.71, 5.21/4.2/2.5, and 29.21/26.67/21.93 mm, respectively. The above findings show the good performance of the proposed CHZ model, especially for Qinghai–Tibet region with the largest height differences in China.

In addition, the comparison between the CHZ model and other typical models published previously is performed. Several Global ZTD models (SHATrop, TropGrid2, IGGtrop_SH, and IGGtrop_rH) and regional ZTD models (AFRC-Trop and DLztd) are selected, and Table VI provides the specific information of compared results for different empirical ZTD models. Analysis of the typical ZTD model published previously reveals

TABLE VI
STATISTICAL RESULT OF ZTD EMPIRICAL MODELS PUBLISHED IN RECENT YEARS

Scale	Studies	Study area	Time length	Time resolution	RMS (cm)	Bias (cm)	Seasonal
Global	GPT2 [19]	Global	2001-2010	1h	9.3	-1.3	No
	TropGrid2 [15]	Global	1999-2008	1h	3.8	-0.3	Yes
	GGZTD [36]	Global	2008-2015	6h	3.58	0.66	No
	GZTD [2]	Global	2002-2009	day	3.9	-0.3	No
	SZTD [48]	Global	2008-2017	6h	4.2	3.0	No
	IGGtrop_SH and IGGtrop_rH [20]	Global	2010-2013	1h	3.8/ 3.9	-0.26/ -0.27	No
Regional	IGGTrop [49]	Europe	2018	1h	3.01	4.5	No
	SHAO-G [50]	China	1997-2007	6h	4.1	-1.2	No
	IGPT2w [47]	China	2015-2017	1h	2.58	1.9	No
	SHATrop [26]	China	2017-2019	3h	3.5	-	Yes
	AFRC-Trop [23]	Africa	2010-2018	1h	3.77	-	No
	DLztd [51]	West Africa	2015-2018	1h	8.22	-	No
	The study	China	2018-2018	1h	2.11	0.25	Yes

*The contents of the table are arranged according to the publication time of the paper.

that the ZTD models are mostly global, which cannot accurately estimate the regional ZTD values, especially for regions with large height differences. In addition, some regional models are established, but the height and season factors are previously poorly considered. However, the CHZ model proposed in this article considers the height and season factors. This model is also established in different regions of China to describe the more sophisticated change in ZTD effectively. Compared with the previous ZTD models, the time resolution of ZTD used for establishing the CHZ model is the highest, and the RMS and Bias of the proposed CHZ model are the smallest. Compared with the global GGZTD and regional IGPT2w models with the highest performance previously, the improvement rates of RMS for the CHZ model are approximately 41.1% and 18.2%, respectively. Such comparisons verify the superiority and good performance of the proposed CHZ model in this article.

E. Application of CHZ Model on PPP

The initial ZTD values derived from GPT3 and CHZ model proposed in this article has been used in PPP, and Fig. 12 gives the positioning errors of simulated PPP technique at four GNSS stations (HAJY, GSPL, QHME, and GSDX) with the time interval of 30 s in N, E, and U directions at March 15, 2018. Those four GNSS stations are selected because they correspond to different heights with values of 2972.1, 1881, 1409.5, and 577.5 m, respectively. Taking the position of four GNSS stations processed by Canadian Spatial Reference System PPP service as the reference, and the thresholds for convergence are 0.1 m and 0.1 m in horizontal and vertical components, respectively [52]. It can be found that CHZ-based PPP has a shorter convergence time than that of GPT3-based PPP in N, E and U components at four GNSS stations with different heights.
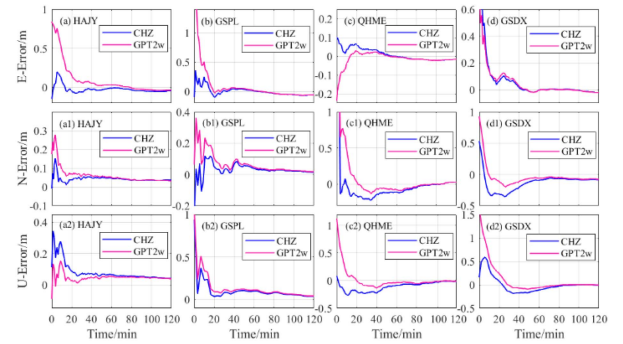

Fig. 12. Comparison of convergence times of different ZTD models at four GNSS stations with different heights in March 15, 2018.

TABLE VII
COMPARISONS OF THE MEAN POSITIONING ERRORS USING DIFFERENT ZTD MODELS IN PPP AT FOUR GNSS STATIONS

Stations	CHZ	GPT2w	CHZ	GPT2w	CHZ	GPT2w
	N/mm		E/mm		U/mm	
QHME	6.1	6.2	-24.3	-24.3	-1.1	1.1
GSDX	7.4	7.6	-20.2	-19.5	0.6	1.1
GSPL	6.1	6.4	-23.9	-23.5	-2.1	-2.4
SXXX	8.6	8.8	-16.5	-16.9	2.5	3.2
Aver.	7.1	7.3	-21.5	-21.1	1.5	2.0

In addition, Tables VII and VIII give the statistical results of the mean positioning errors and convergence time in horizontal and vertical components at selected four GNSS stations, respectively. Here, the real-time precise orbit and clock are recovered

TABLE VIII
COMPARISONS OF CONVERGENCE TIMES USING DIFFERENT ZTD MODELS IN
PPP AT FOUR GNSS STATIONS

Stations	CHZ	GPT2w	CHZ	GPT2w	CHZ	GPT2w
	N/min		E/min		U/min	
QHME	15.5	18	15	27.5	33	38.5
GSDX	9.5	11.5	12	12	10.5	11.5
GSPL	6	12	12	14	7	14
SXXX	7.5	17	17	11.5	12	13.5
Aver.	9.6	14.6	14	16.5	15.6	24.2
Improvement	34%		15%		35%	

using the data provided by Centre National d'Etudes Spatiales, and the convergence time is marked by the deviation of N, E and U components less than 10 cm in 20 consecutive epochs [52]. It can be found that the position accuracy of CHZ-based PPP at four stations is not improved evidently in three components when compared to that from GPT3-based PPP, however, the convergence time of CHZ-based PPP is accelerated to different degrees in horizontal and vertical components due to a high-accuracy priori ZTD can be provided by CHZ model. Statistical results shows that the averaged convergence time of CHZ-based PPP is improved by 34%, 15%, and 35%, respectively, in N, E, and U components when compared to GPT3-based PPP.

V. CONCLUSION

This article proposed a high-precision CHZ to overcome the defect of existing empirical ZTD models that poorly consider the influence of height on ZTD, especially for regions with large height differences. This model considers the influence of height and season on ZTD and is established in accordance with the climatic characteristics of different regions in China to provide more sophisticated descriptions of the ZTD change. In addition, the GPT3 model is used to calculate the initial ZTD value of the CHZ model. The periodical signals of ZTD residual are first determined by the LSP method in each subregion of China, and found that different periodical signals existed in various regions of China. The relationship between ZTD periodical residual and height is then further analyzed, and linear relationships between them are found and used to establish the corresponding function models. Finally, the CHZ-derived ZTD is obtained by adding the ZTD and ZTD periodical residuals to the GPT3-derived ZTD. The corresponding data of 164 GNSS and 87 RS stations over the period of 2012 to 2018 are used for the experiment, and China is divided into four regions (Northwest, North, South, and Qinghai–Tibet) according to the climate characteristics. The experimental result shows that the CHZ model can effectively overcome the impact of height on ZTD and has good internal accuracy with the averaged STD, Bias and MAE of 22.8, 2.1 and 23.8 mm, respectively, in the whole of China. The external validations with GNSS and RS data also demonstrate the superiority and robustness of the proposed CHZ model, especially for Qinghai–Tibet with the largest height difference in China. The averaged RMS, Bias, and MAE of the CHZ model are 21.4/27.0, 2.5/5.1, and 24.9/29.3 mm, respectively, in the whole of China compared with ZTD from the external GNSS and RS stations, respectively. In addition, the comparison with existing empirical ZTD models previously performed and statistical results reveal that the RMS and Bias of the CHZ model are the smallest among these models, which also indicates the good performance of the proposed CHZ model in this article. The application of proposed CHZ model in PPP show the positive improvement in convergence time with improvement rates of 34%, 15%, and 35%, respectively, in N, E, and U components when compared to GPT3-based PPP.

REFERENCES

[1] M. Ding, "Developing a new combined model of zenith wet delay by using neural network," *Adv. Space Res.*, vol. 70, no. 2, pp. 350–359, 2022.
[2] Y. Yao, C. He, B. Zhang, and C. Q. Xu, "A new global zenith tropospheric delay model GZTD," *Chin. J. Geophys.*, vol. 56, no. 7, pp. 2218–2227, 2013.
[3] Y. F. Yang, X. P. Chen, M. H. Yao, C. L. Zhou, and C. M. Liao, "Research on Zenith tropospheric delay modeling of regional CORS network," *Int. Arch. Photogrammetry, Remote Sens. Spatial Inf. Sci.*, vol. 42, pp. 1197–1200, 2020.
[4] J. Saastamoinen, "Atmospheric correction for the troposphere and stratosphere in radio ranging satellites," *Use Artif. Satel. Geodesy*, vol. 15, pp. 247–251, 1972.
[5] H. S. Hopfield, "Two-quartic tropospheric refractivity profile for correcting satellite data," *J. Geophysical Res.*, vol. 74, no. 18, pp. 4487–4499, 1969.
[6] H. S. Hopfield, "Tropospheric effect on electromagnetically measured range: Prediction from surface weather data," *Radio Sci.*, vol. 6, no. 3, pp. 357–367, 1971.
[7] H. D. Black, "An easily implemented algorithm for the tropospheric range correction," *J. Geophysical Res., Solid Earth*, vol. 83, no. B4, pp. 1825–1828, 1978.
[8] Y. Yao, Y. Hu, C. Yu, B. Zhang, and J. Guo, "An improved global zenith tropospheric delay model GZTD2 considering diurnal variations," *Nonlinear Processes Geophys.*, vol. 23, no. 3, pp. 127–136, 2016.
[9] P. Collins, "Assessment and development of a tropospheric delay model for aircraft users of the global positioning system," Univ. New Brunswick, 1999.
[10] P. Collins and R. B. Langley, "Nominal and extreme error performance of the UNB3 tropospheric delay mode1," Dept. of Geodesy and Geomatics Eng., Univ. New Brunswick, Fredericton, Canada, 1999.
[11] P. Collins and R. B. Langley, "Tropospheric delay- Prediction for the WAAS user," *GPS World*, vol. 10, no. 7 pp. 52–58, 1999.
[12] Q. Guo and X. Wu, "A global assessment of ray-traced and blind tropospheric models in the retrieval of tropospheric parameters from ground-based GPS observations," *J. Atmospheric Sol.-Terr. Phys.*, vol. 190, pp. 16–35, 2019.
[13] N. Penna, A. Dodson, and W. Chen, "Assessment of EGNOS tropospheric correction model," *J. Navigation*, vol. 54, no. 1, pp. 37–55, 2001.
[14] E. Krueger and T. Schueler, "Arbesser-Rastburg B. The standard tropospheric correction model for the European satellite navigation system Galileo," in *Proc. Gen. Assem. URSI*, 2005, pp. 23–29.
[15] T. Schüler, "The TropGrid2 standard tropospheric correction model," *GPS Solutions*, vol. 18, no. 1, pp. 123–131, 2014.
[16] J. Böhm, R. Heinkelmann, and H. Schuh, "Short note: A global model of pressure and temperature for geodetic applications," *J. Geodesy*, vol. 81, no. 10, pp. 679–683, 2007.

[17] K. Lagler, M. Schindelegger, J. Böhm, H. Krásná, and T. Nilsson, "GPT2: Empirical slant delay model for radio space geodetic techniques," *Geophysical Res. Lett.*, vol. 40, no. 6, pp. 1069–1073, 2013.

[18] J. Böhm, G. Möller, M. Schindelegger, G. Pain, and R. Weber, "Development of an improved empirical model for slant delays in the troposphere (GPT2w)," *GPS Solutions*, vol. 19, no. 3, pp. 433–441, 2015.

[19] D. Landskron and J. Böhm, "VMF3/GPT3: Refined discrete and empirical troposphere mapping functions," *J. Geodesy*, vol. 92, no. 4, pp. 349–360, 2018.

[20] W. Li, Y. Yuan, J. Ou, and Y. He, "IGGtrop_SH and IGGtrop_rH: Two improved empirical tropospheric delay models based on vertical reduction functions," *IEEE Trans. Geosci. Remote Sens.*, vol. 56, no. 9, pp. 5276–5288, Sep. 2018.

[21] Z. Sun, B. Zhang, and Y. Yao, "A global model for estimating tropospheric delay and weighted mean temperature developed with atmospheric reanalysis data from 1979 to 2017," *Remote Sens.*, vol. 11, no. 16, 2019, Art. no. 1893.

[22] H. Yang, W. Hu, L. YU, X. Nie, and H Li, "GHop: A new regional tropospheric zenith delay model," *Geomatics Inf. Sci. Wuhan Univ.*, vol. 45, no. 2, pp. 226–232, 2020.

[23] M. Abdelazeem, "AFRC-Trop: New real-Time Zenith tropospheric delay model over Africa," *J. Surveying Eng.*, vol. 147, no. 2, 2021, Art. no. 04021003.

[24] J. Dousa and G. V. Bennitt, "Estimation and evaluation of hourly updated global GPS Zenith Total Delays over ten months," *GPS Solutions*, vol. 17, no. 4, pp. 453–464, 2013.

[25] J. Chen, J Wang, J. Wang, and W. Tan, "SHAtrop: Empirical ZTD model based on CMONOC GNSS network," *Geomatics Inf. Sci. Wuhan Univ.*, vol. 44, no. 11, pp. 1588–1595, 2019.

[26] L. Huang, G. Zhu, L. Liu, H. Chen, and W. Jiang, "A global grid model for the correction of the vertical zenith total delay based on a sliding window algorithm," *GPS Solutions*, vol. 25, no. 3, pp. 1–14, 2021.

[27] D. Dong, G. Huang, X. Qu, W. Tao, and G. Fan, "Temperature trend–altitude relationship in China during 1963–2012," *Theor. Appl. Climatol.*, vol. 122, no. 1, pp. 285–294, 2015.

[28] L. Huang et al., "High-precision GNSS PWV retrieval using dense GNSS sites and in-situ meteorological observations for the evaluation of MERRA-2 and ERA5 reanalysis products over China," *Atmospheric Res.*, vol. 276, 2022, Art. no. 106247.

[29] O. Bothe, K. Fraedrich, and X. Zhu, "Precipitation climate of Central Asia and the large-scale atmospheric circulation," *Theor. Appl. Climatol.*, vol. 108, no. 3, pp. 345–354, 2012.

[30] J. Fang, G. Yu, L. Liu, S. Hu, and F. S. Chapin III, "Climate change, human impacts, and carbon sequestration in China," *Proc. Nat. Acad. Sci.*, vol. 115, no. 16, pp. 4015–4020, 2018.

[31] H. Zhang, Y. Yuan, and W. Li, "An analysis of multisource tropospheric hydrostatic delays and their implications for GPS/GLONASS PPP-based zenith tropospheric delay and height estimations," *J. Geodesy*, vol. 95, no. 7, pp. 1–19, 2021.

[32] O. A. Isioye, L. Combrinck, and J. Botai, "Evaluation of spatial and temporal characteristics of GNSS-derived ZTD estimates in Nigeria," *Theor. Appl. Climatol.*, vol. 132, no. 3, pp. 1099–1116, 2018.

[33] T. A. Herring, R. W. King, and S. C. McClusky, *Documentation of the GAMIT GPS Analysis Software Release 10.4; Department of Earth and Planetary Sciences*. Cambridge, MA, USA: Massachusetts Inst. of Technol., 2010, pp. 1–171.

[34] Z. Altamimi, X. Collilieux, and L. Métivier, "ITRF2008: An improved solution of the international terrestrial reference frame," *J. Geod.*, vol. 85, pp. 457–473, 2011.

[35] Q. Zhao, P. Yang, W. Yao, and Y. Yao, "Hourly PWV dataset derived from GNSS observations in China," *Sensors*, vol. 20, no. 1, pp. 1–16, 2019a.

[36] Q. Zhao, Y. Yao, X. Cao, F. Zhou, and P. Xia, "An optimal tropospheric tomography method based on the multi-GNSS observations," *Remote Sens.*, vol. 10, no. 2, pp. 1–15, 2018.

[37] L. Huang, H. Chen, L. Liu, and W. Jiang, "A new high-precision global model for calculating zenith tropospheric delay," *Chin. J. Geophys.*, vol. 64, no. 3, pp. 782–795, 2021.

[38] J. Askne and H. Nordius, "Estimation of tropospheric delay for microwaves from surface weather data," *Radio Sci.*, vol. 22, no. 3, pp. 379–386, 1987.

[39] I. Durre, R. S. Vose, and D. B. Wuertz, "Overview of the integrated global radiosonde archive," *J. Climate*, vol. 19, no. 1, pp. 53–68, 2006.

[40] F. Ahmed, P. Vaclavovic, F. N. Teferle, J. Douša, R. Bingley, and D. Laurichesse, "Comparative analysis of real-time precise point positioning zenith total delay estimates," *GPS Solutions*, vol. 20, no. 2, pp. 187–199, 2016.

[41] J. S. Haase, H. Vedel, M. Ge, and E. Calais, "GPS zenith tropospheric delay (ZTD) variability in the Mediterranean," *Phys. Chem. Earth, A, Solid Earth Geodesy*, vol. 26, no. 6–8, pp. 439–443, 2001.

[42] W. Suparta, A. Iskandar, M. S. J. Singh, M. A. M. Ali, B. Yatim, and A. N. M. Yatim, "Analysis of GPS water vapor variability during the 2011 La Niña event over the western Pacific Ocean," *Ann. Geophys.*, vol. 56, no. 3, 2013, Art. no. R0330.

[43] J. D. Scargle, "Studies in astronomical time series analysis. II-Statistical aspects of spectral analysis of unevenly spaced data," *Astrophysical J.*, vol. 263, pp. 835–853, 1982.

[44] M. Ding, W. Hu, X. Jin, and L. Yu, "A new ZTD model based on permanent ground-based GNSS-ZTD data," *Surv. Rev.*, vol. 48, no. 351, pp. 385–391, 2016.

[45] Q. Zhao, Y. Yao, W. Yao, and S. Zhang, "GNSS-derived PWV and comparison with radiosonde and ECMWF ERA-Interim data over mainland China," *J. Atmospheric Sol.-Terr. Phys.*, vol. 182, pp. 85–92, 2019b.

[46] P. Wei, S. Xie, L. Huang, and L. Liu, "Ingestion of GNSS-Derived ZTD and PWV for spatial interpolation of PM2. 5 concentration in Central and Southern China," *Int. J. Environ. Res. Public Health*, vol. 18, no. 15, 2021, Art. no. 7931.

[47] Z. Du, Q. Zhao, W. Yao, and Y. Yao, "Improved GPT2w (IGPT2w) model for site specific zenith tropospheric delay estimation in China," *J. Atmospheric Sol.-Terr. Phys.*, vol. 198, 2020, Art. no. 105202.

[48] J. Mao, Q. Wang, Y. Liang, and T. Cui, "A new simplified zenith tropospheric delay model for real-time GNSS applications," *GPS Solutions*, vol. 25, no. 2, pp. 1–12, 2021.

[49] W. Li, Y. B. Yuan, J. K. Ou, H. Li, and Z. S. Li, "A new global zenith tropospheric delay model IGGtrop for GNSS applications," *Chin. Sci. Bull.*, vol. 57, no. 17, pp. 2132–2139, 2012.

[50] Q. Chen, S. Song, and W. Zhu, "An analysis for the accuracy of tropospheric zenith delay calculated from ECMWF/NCEP data over Asia," *Chin. J. Geophys.*, vol. 55, no. 3, pp. 275–283, 2012.

[51] S. Osah, A. A. Acheampong, C. Fosu, and I. Dadzie, "Deep learning model for predicting daily IGS zenith tropospheric delays in West Africa using tensorflow and keras," *Adv. Space Res.*, vol. 68, no. 3, pp. 1243–1262, 2021.

[52] P. Collins, S. Bisnath, F. Lahaye, and P. Héroux, "Undifferenced GPS ambiguity resolution using the decoupled clock model and ambiguity datum fixing," *Navigation*, vol. 57, no. 2, pp. 123–135, 2010.

Qingzhi Zhao received the B.Sc. degree from Shandong Agricultural University, Taian, China, in 2011, the M.Sc. degree from China University of Mining and Technology, Xuzhou, China, in 2014, and Ph.D. degree from Wuhan University, Wuhan, China, in 2017, all in geodesy and surveying engineering.

He is an Associate Professor with the Xi'an University of Science and Technology, Xi'an, China. His research interests include GNSS data processing and GNSS meteorology.

Jing Su received the B.Sc. degree in geodesy and surveying engineering from Xi'an University of Science and Technology, Xi'an, China, in 2020, where she is currently working toward the master's degree in geodesy and surveying engineering.

Her research interest includes GNSS Meteorology.

Chaoqian Xu received the B.Sc., master's, and Ph.D. degrees in geodesy and surveying engineering from Wuhan University, Wuhan, China, in 2007, 2013, and 2017, respectively.

He is currently an Associate Professor with Wuhan University. His main research interests include global navigation satellite system meteorological studies, theory, and method of establishing high-precision ZTD model.

Xiaoya Zhang received the B.Sc. degree in resources and environmental from the Henan University of Urban Construction, Pingdingshan, China, in 2021, where he is currently working toward the master's degree in geodesy and surveying engineering.

His research interest includes GNSS Meteorology.

Yibin Yao received the B.Sc., master's, and Ph.D. degrees (with distinction) in geodesy and surveying engineering from Wuhan University, Wuhan, China, in 1997, 2000, and 2004, respectively.

He is currently a Professor with Wuhan University. His main research interests include global navigation satellite system ionospheric/atmospheric/ meteorological studies, theory and method of surveying data processing, and GPS/MET and high-precision GPS data processing.

Jifeng Wu received the B.Sc., master's, and Ph.D. degrees in geodesy and surveying engineering from Chang'an University, Xi'an, China, in 2008, 2012, and 2016, respectively.

His main research interests include global navigation satellite system and its innovative application.